From thermodynamic cell models to partitioning cellular automata for diffusion in zeolites. II. Static and dynamic properties

ARTICLE *in* THE JOURNAL OF CHEMICAL PHYSICS · DECEMBER 2009

Impact Factor: 2.95 · DOI: 10.1063/1.3267636 · Source: PubMed

3 AUTHORS:

Federico G Pazzona
Università degli Studi di Sassari
28 PUBLICATIONS **159** CITATIONS
SEE PROFILE

Pierfranco Demontis
Università degli Studi di Sassari
123 PUBLICATIONS **2,172** CITATIONS
SEE PROFILE

Giuseppe B Suffritti
Università degli Studi di Sassari
133 PUBLICATIONS **2,106** CITATIONS
SEE PROFILE

From thermodynamic cell models to partitioning cellular automata for diffusion in zeolites. II. Static and dynamic properties

Federico G. Pazzona, Pierfranco Demontis, and Giuseppe B. Suffritti

Citation: J. Chem. Phys. **131**, 234704 (2009); doi: 10.1063/1.3267636
View online: http://dx.doi.org/10.1063/1.3267636
View Table of Contents: http://jcp.aip.org/resource/1/JCPSA6/v131/i23
Published by the AIP Publishing LLC.

From thermodynamic cell models to partitioning cellular automata for diffusion in zeolites. II. Static and dynamic properties

Federico G. Pazzona,[a] Pierfranco Demontis,[b] and Giuseppe B. Suffritti
Dipartimento di Chimica, Università degli Studi di Sassari and Consorzio Interuniversitario Nazionale per la Scienza e Tecnologia dei Materiali (INSTM), Unità di Ricerca di Sassari, via Vienna, 2, I-07100 Sassari, Italy

(Received 17 September 2009; accepted 4 November 2009; published online 17 December 2009)

In this second paper we exploit our thermodynamic partitioning cellular automaton (PCA) developed in Paper I [Pazzona *et al.*, J. Chem. Phys. **131**, 234703 (2009)] to study *interacting* molecules adsorbed in microporous materials. We present a mean-field theory of the single cell model at equilibrium followed by a detailed description of the procedure we propose to calculate the chemical potential in the canonical ensemble. Finally we use our approach to simulate transport properties starting from the parameterization devised by Ayappa [J. Chem. Phys. **111**, 4736 (1999)] to reproduce the adsorption properties of xenon in zeolite NaA. We report how the correlations included in the PCA evolution rule affect the estimated self-diffusion coefficient. © *2009 American Institute of Physics*. [doi:10.1063/1.3267636]

I. INTRODUCTION

A cellular automaton (CA)[1–3] is a stylized universe where simple, local evolution rules generate discrete observables in a discrete space of cells. The discrete-time evolution of such observables constitutes the CA *microdynamics*. Due to its discreteness, the CA microdynamics cannot be realistic in the strictest sense, but becomes meaningful once the statistical properties, averaged over a sufficiently long observation time, are extracted from a simulation. This suggests the use of a CA framework to model a *coarse-grained* version of a detailed (e.g., atomistic) system. Through opportune setting of the CA constitutive parameters, statistical agreement with the system to be emulated can be achieved *on a selected scale*. As an example, when considering the problem of adsorption/diffusion of simple adsorbates in regular microporous materials such as zeolites (a good coarse-grained representation of which can be easily modeled under the framework of a CA[4–6]), connection with the largest space-time scales is established once agreement of adsorption isotherm and diffusivity profile has been obtained. The CA's statistical realism can be further improved by increasing the level of detail in description of space and evolution rule, in order to mimic, e.g., the stationary density distributions and correlations in the particles' motion observed in atomistic simulations. As in any other coarse-graining framework, smaller are the scales one wants to recover, many more are the hierarchical levels to be introduced in the CA structure.

The formulation of proper thermodynamic models with very local interactions has been proved to be very useful in the description of equilibrium thermodynamic properties of adsorption systems (see Cheung[7] and Ayappa[8]), while providing no information about the dynamics of transfer processes associated to adsorption. On the other hand, equilibrium and nonequilibrium kinetic Monte Carlo (KMC) models have been developed to capture diffusion properties on adsorption materials through effective transfer rates from pore to pore under a coarse-grained approach.[9–13] The KMC approach usually tracks the motion of one molecule, subject to interactions with the microporous medium and possibly with other molecules, rather than of a whole set of molecules. Therefore thermodynamic properties involving the detection of more than one molecule's position at a time cannot be evaluated through KMC. Examples are the distribution of pore occupancies at a given loading, the persistence time of a given pore occupancy in a zeolite, or the collective diffusion coefficient.

In the preceding companion paper, denoted as Paper I,[30] we developed in detail the theoretical basis of our thermodynamic partitioning CA (PCA) devised as a dynamical evolution of static thermodynamic cell models.[7,8] In this second paper the foundations of a mean-field theory of the single cell at equilibrium will be presented in Sec. II, followed by a short illustration of the way the chemical potential can be calculated in our model in Sec. III. Finally, in Sec. IV we shall use our PCA approach to simulate transport properties starting from a model constructed by Ayappa[8] to reproduce the adsorption properties of xenon in zeolite NaA, then we shall discuss the effect of correlations on the estimated self-diffusion coefficient.

II. SINGLE CELL AT EQUILIBRIUM: GRAND-CANONICAL FORMULATION

The thermodynamic approach allows a mean-field theory to be developed for our PCA under the assumption that occupancies are distributed in the neighborhood of an n-occupied cell according to the same occupancy probability distribution of the entire system. Such a distribution, denoted

[a]Present address: National Technical University of Athens, School of Chemical Engineering, 9 Heroon Polytechniou Street, 15780 Athens, Greece.
[b]Electronic mail: demontis@uniss.it.

$\mathbf{p}=\{p(n)\}_{n=0,\ldots,K}$ (where $p(n)$ is the probability of a cell to be occupied by n particles), depends on the loading (average occupancy) $\langle n\rangle=N/M$. Each loading is related to a particular value of the chemical potential μ according to the *adsorption isotherm* of the system. While in numerical simulations of PCA $\langle n\rangle$ is constant, in the mean-field approach it is appropriate to work with constant μ_{GC} [where the subscript GC emphasizes that we are dealing with the grand-canonical ensemble (GCE)]. In order to establish a connection between the statistics of the GCE and the thermodynamics of our PCA we compute the occupancy distribution as[14]

$$p(n)=\frac{Q(n)e^{\beta\mu n}}{\Xi(\mu)}, \tag{1}$$

where $Q(n)$ is the canonical partition function for a closed cell of occupancy n and the denominator,

$$\Xi(\mu)=\sum_{n=0}^{K}Q(n)e^{\beta\mu n}, \tag{2}$$

is the grand-canonical partition function of the open cell. It emerges that to evaluate the grand partition function we have to pass through the evaluation of the canonical partition function. Under the above mentioned assumption of an *homogeneous distribution of occupancies*, the core of our mean-field theory, we find that an explicit evaluation of $Q(n)$ is quite easy proving the value of the developed formalism. The loading, $\langle n\rangle$, and the occupancy variance, $\langle n^2\rangle-\langle n\rangle^2$, can then be recovered through the first and second moment of $p(n)$

$$\langle n\rangle=\sum_{n=0}^{K}np(n)=\frac{1}{\beta}\frac{\partial\ln\Xi(\mu)}{\partial\mu}, \tag{3}$$

$$\langle n^2\rangle-\langle n\rangle^2=\sum_{n=0}^{K}(n-\langle n\rangle)^2p(n)=\frac{1}{\beta}\frac{\partial\langle n\rangle}{\partial\mu}. \tag{4}$$

We define the *intercell transfer factor* $W(n,m)$ as the conditional probability to observe a transfer of a particle from cell L to cell R given that their occupancies are n and m, respectively,

$$W(n,m)=\frac{1}{K_{ex}^2}\sum_{n_{ex}=0}^{K_{ex}}\sum_{m_{ex}=0}^{K_{ex}}n_{ex}(K_{ex}-m_{ex})\times P(n_{ex}|n)P(m_{ex}|m)p^P(n_{ex},n,m_{ex},m), \tag{5}$$

defined for $n=1,\ldots,K$ and $m=0,\ldots,K-1$, where K_{ex} is the number of exit sites per cell and p^P is the propagation acceptance for a particle jumping from an n-occupied cell with n_{ex} occupied exit sites (including the jumping particle) to an m-occupied cell with m_{ex} occupied exit sites, defined as

$$p^P(n_{ex},n,m_{ex},m)=\frac{e^{-\beta\epsilon_{ki}(n,m)}}{1+e^{\beta\Delta F(n_{ex},n,m_{ex},m)}}. \tag{6}$$

The probabilities P and p^P have been defined in Paper I,[30] Eqs. (31) and (53). In Eq. (6) the term

$$\Delta F(n_{ex},n,m_{ex},m)=\Phi(n_{ex}-1,n-n_{ex})+\Phi(m_{ex}+1,m-m_{ex})-\Phi(n_{ex},n-n_{ex})-\Phi(m_{ex},m-m_{ex}), \tag{7}$$

is the free energy difference between the pre- and the post-propagation state. From the occupancy distribution and the intercell transfer factor we can derive the equilibrium probability of a particle to escape from its current cell as

$$p^{esc}=\frac{K_{ex}}{\langle n\rangle}\sum_{n=1}^{K}\sum_{m=0}^{K-1}p(n)p(m)W(n,m), \tag{8}$$

which is the reciprocal of the average number of subsequent time steps during which a particle stays in the same cell, i.e.,

$$\tau_{mrt}=\tau/p^{esc}, \tag{9}$$

where τ_{mrt} is the mean residence time of a particle in a cell (in units of seconds), and τ is the duration of a time step (in seconds as well) which is discussed in Appendix A.

In order to define the mean-field self-diffusivity we introduce the *instantaneous cell-to-cell displacement* of a single particle

$$\delta\mathbf{r}(t)=\lambda\sum_{j=1}^{2d}\varphi_j(t)\mathbf{e}_j, \tag{10}$$

where $\boldsymbol{\varphi}(t)=\{\varphi_j(t)\}_{j=1,\ldots,2d}$ is a Boolean vector satisfying the following property:

$\varphi_j(t)=1,0$ whether the particle undergoes or not propagation from its current cell, say $\mathbf{r}$, to its jth neighboring cell, i.e., $\mathbf{r}^j$, at time t.

Its total displacement at time t (i.e., after $Z=t/\tau$ time steps) is given by

$$\Delta\mathbf{r}(t)=\sum_{z=0}^{Z-1}\delta\mathbf{r}(z\tau), \tag{11}$$

and its mean square displacement is given by

$$\langle[\Delta\mathbf{r}(t)]^2\rangle=\left\langle\sum_{z=0}^{Z-1}\sum_{z'=0}^{Z-1}\delta\mathbf{r}(z\tau)\cdot\delta\mathbf{r}(z'\tau)\right\rangle, \tag{12}$$

where z,z' denote time steps. By expanding the sum in Eq. (12) and using the Einstein relation for the self-diffusivity, which for a discrete-time evolution reads

$$D_s=\frac{1}{2d}\lim_{t\to\infty}\frac{\langle[\Delta\mathbf{r}(t+\tau)]^2\rangle-\langle[\Delta\mathbf{r}(t)]^2\rangle}{\tau}, \tag{13}$$

we get the Green–Kubo type formula for the self-diffusion coefficient in the (hyper)cubic PCA, in terms of the instantaneous displacement $\delta\mathbf{r}(t)$ instead of velocity[15]

$$D_s=\frac{1}{2d\tau}\left[\langle\delta\mathbf{r}(0)\cdot\delta\mathbf{r}(0)\rangle+2\sum_{z=1}^{\infty}\langle\delta\mathbf{r}(z\tau)\cdot\delta\mathbf{r}(0)\rangle\right], \tag{14}$$

where we have separated the contribution at equal times from the correlations between different times. In Eq. (14), $z\tau$ (with $z=0,1,2,\ldots$) represents the discrete PCA time $t=0,\tau,2\tau,\ldots$. The quantity $\tau^{-2}\langle\delta\mathbf{r}(z\tau)\cdot\delta\mathbf{r}(0)\rangle$ in Eq. (14) is

the analogous of the velocity autocorrelation function for a continuous system. In particular its value at $z=0$, i.e., $\langle \delta\mathbf{r}(0)\cdot\delta\mathbf{r}(0)\rangle$ is λ^2 times the escape probability given in Eq. (8). where we have separated the contribution at equal times from the correlations between different times. The quantity $\tau^{-2}\langle \delta\mathbf{r}(t)\cdot\delta\mathbf{r}(0)\rangle$ in Eq. (14) is the analogous of the velocity autocorrelation function for a continuous system. In particular its value at $t=0$, i.e., $\langle \delta\mathbf{r}(0)\cdot\delta\mathbf{r}(0)\rangle$ is λ^2 times the escape probability given in Eq. (8). If we make the assumption of uncorrelated motion then the summation in Eq. (14) is null and we obtain for the mean-field self-diffusivity

$$D_0^{\mathrm{mf}} = \frac{\lambda^2}{\tau}\frac{K_{\mathrm{ex}}}{2d\langle n\rangle}\sum_{n=1}^{K}\sum_{m=0}^{K-1} p(n)p(m)W(n,m), \tag{15}$$

which turns out to be related with the mean residence time introduced in Eq. (9) according to $D_0^{\mathrm{mf}}=\lambda^2/2d\tau_{\mathrm{mrt}}$. The quantity D_0^{mf} is exactly the *memoryless diffusivity* (see Paper I[30]) produced in numerical simulations where the memoryless randomization is used.

The introduction of backscattering correlations in the self-motion by means of the jump randomization operator $\mathcal{R}^{\mathrm{jump}}$ causes the value of D_s obtained from numerical simulations to strongly deviate from D_0^{mf}. In Sec. IV such correlation effects will be studied by means of numerical simulations under different conditions.

III. EVALUATION OF CHEMICAL POTENTIAL FROM NUMERICAL SIMULATIONS

Widom[16] test particle method is widely used in atomistic simulations to calculate chemical potential. Its statistical mechanical basis rests on the change a system's Helmholtz free energy has in the canonical ensemble by adding a virtual particle. Then the chemical potential can be calculated by the increment of free energy, meaning that chemical potential is just related to the increase in system's Helmholtz free energy before and after adding a virtual particle. Here we will exploit this strategy to show how a formulation for the chemical potential of our PCA can be constructed as a function of the local partition function and the occupancy distribution defined in Eq. (1), without performing any insertion-deletion move during the simulation: The starting relations are

$$p(n+1) = \Xi(\mu)^{-1}e^{\beta\mu}Q(n+1)e^{\beta\mu n}, \quad n=0,\ldots,K-1 \tag{16}$$

and

$$p(n-1) = \Xi(\mu)^{-1}e^{-\beta\mu}Q(n-1)e^{\beta\mu n}, \quad n=1,\ldots,K, \tag{17}$$

which can be combined individually with Eq. (1) to give, respectively, an *insertion formula*

$$e^{-\beta\mu} = \frac{Q(n+1)}{Q(n)}\frac{p(n)}{p(n+1)}, \quad n=0,\ldots,K-1, \tag{18}$$

and a *deletion formula*

$$e^{-\beta\mu} = \frac{Q(n)}{Q(n-1)}\frac{p(n-1)}{p(n)}, \quad n=1,\ldots,K, \tag{19}$$

where the partition function Q is calculated as described in Paper I.[30] If the values of the distribution $\mathbf{p}$ are calculated through the mean-field relation, which essentially ignores fluctuations and treats all quantities by their average value, as in Eq. (1), then the two quantities in Eqs. (18) and (19) are perfectly identical. Due to the finite size of the system (that in our case means N particles distributed in M cells) and to the finite duration of the simulation, each value $p_N(n)$ of the occupancy distribution $\mathbf{p}_N$ calculated through numerical simulations is affected by some uncertainty, causing it to differ from the mean-field value $p(n)$. Therefore, if the output of a (long but finite) simulation is used to compute the occupancy distribution $\mathbf{p}_N$, then we will have that $\mathbf{p}_N\approx\mathbf{p}$, and not only the chemical potential estimations calculated through Eqs. (18) and (19) will be different from each other, but also each formula will return values which will depend on the occupancy n. Although the difference is small for a sufficiently long simulation of a large system (e.g., 10^5 time steps for a $16\times16\times16$ system), a proper criterion is needed to obtain one average value of chemical potential. By calculating the mean value of the left-hand side of Eq. (18) we get

$$\bar{A}_{\mathrm{ins}} = \sum_{n=0}^{K-1}\frac{Q(n+1)}{Q(n)}\frac{p_N^2(n)}{p_N(n+1)}, \tag{20}$$

where "ins" stands for an hypothetical "insertion" move, while with Eq. (19) we obtain

$$\bar{A}_{\mathrm{del}} = \sum_{n=1}^{K}\frac{Q(n)}{Q(n-1)}p_N(n-1), \tag{21}$$

where "del" stands for "deletion." The mean chemical potentials related with Eqs. (20) and (21) are $\bar{\mu}_{\mathrm{ins}}=-\beta^{-1}\ln\bar{A}_{\mathrm{ins}}$ and $\bar{\mu}_{\mathrm{del}}=-\beta^{-1}\ln\bar{A}_{\mathrm{del}}$. Both formulations will produce the correct chemical potential for intermediate loadings. For small loadings Eq. (21) becomes inappropriate since empty cells (allowing no deletion moves) become frequent, whereas for high loadings the probability of saturated cells (allowing no insertion moves) increases making Eq. (20) inadequate. Therefore our choice is

$$\exp\{-\beta\bar{\mu}\} = \sum_{n=1}^{K}\frac{n}{K}\frac{Q(n)}{Q(n-1)}p_N(n-1) + \sum_{n=0}^{K-1}\left(1-\frac{n}{K}\right)\frac{Q(n+1)}{Q(n)}\frac{p_N^2(n)}{p_N(n+1)}, \tag{22}$$

which, in one expression, weights properly both insertion and deletion. The prefactors n/K and $(1-n/K)$ take account of the fact that a less occupied cell would preferably undergo a deletion rather than an insertion, and vice versa for a more occupied cell. Indeed in an hypothetical deletion mechanism a site would be randomly picked so that the probability of the deletion move to be performed would be n/K. Likewise, in an hypothetical insertion move the probability to randomly pick an empty site to put one additional particle in would be $(1-n/K)$.

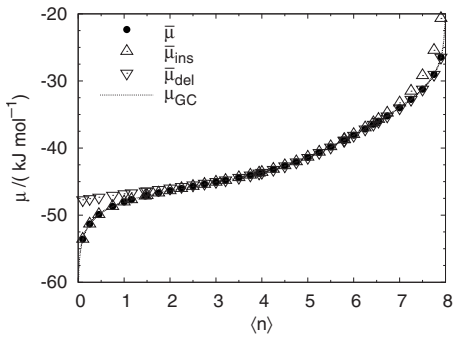

FIG. 1. Modeled chemical potential (units of kJ mol^{-1}) for adsorption of xenon in NaA zeolite at 300 K (Ref. 17). Mean chemical potentials extracted from numerical simulations are plotted together with the chemical potential expected from the grand-canonical formulation of the single cell (see Sec. II), indicated as μ_{GC}.

In a recent paper[17] we modeled the value of K and the free energy parameters $f_{ex}(n)$ and $f_{in}(n)$ from measurements taken by Jameson *et al.*[18,19] so as to emulate the static equilibrium properties of xenon adsorption in NaA zeolite. In Fig. 1 the chemical potential from numerical simulations (in the canonical ensemble) is shown as derived by using Eqs. (20)–(22) and compared to the mean-field value obtained from Eq. (1).

IV. RESULTS AND DISCUSSION

A. Modeling of diffusion on a static thermodynamic model

In this section we shall explore the possible dynamical behaviors that can be modeled on our PCA. First of all we implement the local thermodynamic model constructed by Ayappa[8] for adsorption of xenon in NaA zeolite at 360 K. Following his approach we make use of an energy function of the form

$$E(n) = n\varepsilon^o + \frac{zn^2\varepsilon^{pp}(n)}{2K}, \tag{23}$$

where ε^o is the adsorbate-lattice interaction energy, z is the assumed number of nearest-neighbors per lattice site, and $\varepsilon^{pp}(n)$ is the adsorbate-adsorbate interaction parameter given by the following Lennard-Jones-like functional form

$$\varepsilon^{pp}(n) = 4\epsilon^{lj}\left[\left(\frac{\sigma}{r(n)}\right)^{12} - \left(\frac{\sigma}{r(n)}\right)^{6}\right], \tag{24}$$

with

$$r(n) = (r_2 - r_1)\frac{n}{K} + r_2. \tag{25}$$

In Eqs. (24) and (25), ϵ^{lj} and σ are, respectively, the Lennard-Jones energy parameter and molecular diameter, $r_2 = 2^{1/6}\sigma$, and r_1 is a free parameter.

The effective site volume $v(n)$ changes with the occupancy according to

$$v(n) = v_0\left[\frac{1}{2}\left(\frac{l-\sigma}{2R} + 1\right)^2\right]^{zn/2K}, \tag{26}$$

where v_0 is the volume of the adsorption site associated with a single adsorbate in the absence of neighboring adsorbates, R is the site radius obtained by assuming a cubic site of volume v_0, and l is the lattice parameter. The resulting partition function of an n-occupied cell can be written as

$$Q^{Ay}(n) = e^{-\beta n\phi^{Ay}(n)}\binom{K}{n}e^{-\beta n\varepsilon^o}, \tag{27}$$

where $\phi^{Ay}(n)$ is the interaction free energy term given by

$$\phi^{Ay}(n) = -\frac{1}{\beta}\ln\frac{v(n)}{\Lambda^3} + \frac{zn\varepsilon^{pp}(n)}{2K}. \tag{28}$$

In the application to the problem of xenon adsorption in NaA zeolite, Ayappa[8] assumed $K=12$, $z=4$, $T=360$ K, $\sigma=4.10$ Å, $\varepsilon=-25.6$ kJ mol^{-1}, $\epsilon^{lj}=1.837$ kJ mol^{-1}, $r_2=3.906$ Å, $v_0=7.465$ $Å^3$, and $l=3.58$ Å.

In Eqs. (23)–(27) inner and exit sites are equivalent. However, due to the heterogeneity of the zeolite's cage structure, multiple types of adsorption site differing in adsorption energy are present.[12,20–22] In our line of reasoning this causes the probability of a particle to occupy locations close to the windows to be generally different from the probability to occupy any other location in the cell.[23] In the PCA paradigm such a differentiation is mimicked through the modeling of the difference in statistical weights between exit and inner sites. Such a modeling fosters a dynamics characterized by a hierarchy criterion to decide which particles must be promoted to the exit sites in order to leave their host cell. In this way the attitude of the cells to transmit their content outside becomes strictly dependent on local conditions. Just as observed in zeolites, where the complexity of adsorbate-framework and adsorbate-adsorbate interactions often causes the trends of diffusivity versus loading to be highly nontrivial, the dependence of transport properties of the model on macroscopic observables results to be generally nonlinear.

The PCA paradigm can be used to extend a static thermodynamic model as the one of Ayappa[8] to the simulation of transport properties by assuming two fixed site free-energies, f^o_{ex} and f^o_{in}, entering a cellular partition function of the form

$$Q(n) = e^{-\beta n\phi(n)}Q^o(n), \tag{29}$$

where

$$Q^o(n) = \sum_{n_{ex},n_{in}}^{(n)}\prod_{\alpha=ex,in}\binom{K_\alpha}{n_\alpha}e^{-\beta n_\alpha f^o_\alpha} \tag{30}$$

(see Paper I[30] for the meaning of the superscript $^{(n)}$ on the summation symbol) and $\phi(n)$, $n=1,\ldots,K$ ensures equivalence of Eq. (29) with Eq. (27) through

$$\phi(n) = \phi^{Ay}(n) + \varepsilon^o + \frac{1}{n\beta}\left[\ln Q^o(n) - \ln\binom{K}{n}\right]. \tag{31}$$

Obviously the contents of Eqs. (29)–(31) means to assume $\phi_{ex}(n)=\phi_{in}(n)\equiv\phi(n)$ for each n. Although as a result the trend of $\langle n_{ex}(n)\rangle$ versus n will depend only on the difference

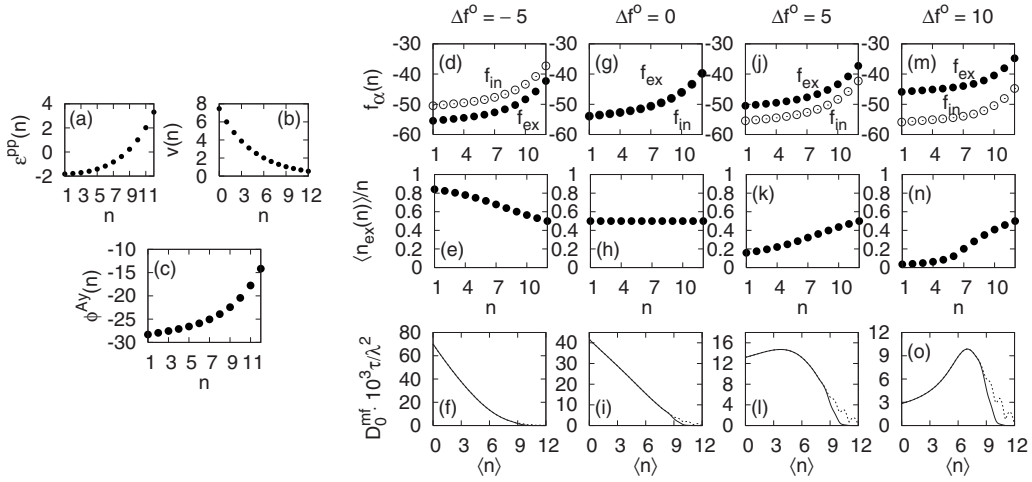

FIG. 2. Possible diffusive behaviors modeled on the thermodynamic model of Ayappa (Ref. 8) for adsorption of xenon in NaA zeolite at 360 K. On the left, an effective interaction free energy function $\phi(n)$ is constructed starting from the given effective Lennard-Jones interaction potential $\varepsilon^{\mathrm{lj}}(n)$ and volume $v(n)$. On the right, four different balances between average occupancies of exit and inner sites are assumed by varying the difference of $\Delta f^o = f^o_{\mathrm{ex}} - f^o_{\mathrm{in}} = -5$, 0, 5 and 10 kJ mol^{-1}. For each column relative to each value of Δf^o, we plotted: (top) The effective site energy profiles $f_{\mathrm{ex}}(n)$ and $f_{\mathrm{in}}(n)$ in units of kJ mol^{-1} vs the occupancy n; (middle) The average exit sites occupancy $\langle n_{\mathrm{ex}}(n)\rangle$; (bottom) The mean-field self-diffusivity D_s^{mf} vs the loading $\langle n\rangle$. Solid and dashed lines represent D_s^{mf}, respectively, with and without the kinetic barrier introduced in Paper I (see Ref. 30). See text of Sec. IV A for further details.

$$\Delta f^o = f^o_{\mathrm{ex}} - f^o_{\mathrm{in}}, \tag{32}$$

and not on the interaction parameter ϕ that assumption will be enough to show the most general diffusion profiles that are available in the PCA parameter space. Anyway, a finer tuning of the transport properties can be acquired through a distinction of the $\phi_{\mathrm{ex}}(n)$ and $\phi_{\mathrm{in}}(n)$ trends, while preserving (numerically) the total value of $Q(n)$, thus enlarging the range of possible dynamical behaviors of the model.

In the left side of Fig. 2 it is shown how local interactions and effective volume are embedded together onto the effective interaction free energy ϕ^{Ay}. In the right side we show how different values of Δf^o generate different transport properties. In details are the following:

(i) In the first line we show how the local free energy parameters, $f^o_{\mathrm{ex}}(n)$ and $f^o_{\mathrm{in}}(n)$, are modified by adapting the cell thermodynamics to different values of Δf^o by means of Eq. (31).

(ii) In the second line a mesoscopic quantity, the *average exit sites accessibility*, given by the ratio $\langle n_{\mathrm{ex}}(n)\rangle/n$ [where $\langle n_{\mathrm{ex}}(n)\rangle$ is the average number of occupied exit sites in a n-occupied cell (with $n=1,\ldots,K$)], is shown for each value of Δf^o. This quantity is of great importance, since it definitely determines the qualitative trend of the memoryless diffusivity.

(iii) In the third line the resulting memoryless diffusivity is shown. Solid lines are obtained through a test modeling of the harmonic force constant $k(n)$ introduced in Paper I,[30] where the jump barrier for jumps between highly occupied cells has been lowered by assuming

$$k(n) = C_1 + (C_2 + C_3 n')n'\theta(n'-1), \tag{33}$$

where $n' = n - \xi + 1$ and the Heaviside function $\theta(x)$ (which has value 1 for $x \geq 0$ and 0 otherwise) allows $k(n)$ to remain constant (and equal to C_1) for occupancies $0 \leq n \leq \xi - 1$, and rises quadratically for $\xi \leq n \leq K-1$. In the example of Fig. 2 we chosen $C_1=0$, $C_2=2$, $C_3=20$, and $\xi=9$. Dotted lines are instead diffusivities obtained with no modeling of the kinetic barrier, i.e., $k=0$.

It should be noted that the choice of Δf^o determines the qualitative shape of the exit sites accessibility (which is a local equilibrium property), which in turn induces a specific qualitative trend of the self-diffusivity (a global equilibrium property). In general, the diffusivity trend embeds the accessibility trend together with the effect of repulsion at high loadings. Since according to Eqs. (8), (9), and (15) the quantity D_s^{mf} is $\lambda^2/2d\tau$ times the escape probability p^{esc}, such trends can be easily explained.

If $\Delta f^o < 0$ [so that the exit sites are deeper than the inner sites, see Figs. 2(d)–2(f)] then the exit sites accessibility exhibits a *decreasing* trend from high values at $n=0$ to K_{ex}/K at $n=K$. Due to the high accessibility, the exit sites are very frequently visited so that during propagation there is a high probability of two adjacent exit sites to be simultaneously occupied. This gives no transfer between the two respective cells. As a consequence, the D_0^{mf} trend will be *decreasing*.

If exit and inner sites are equivalent [i.e., $\Delta f^o=0$, see Figs. 2(g)–2(i)] then $\langle n_{\mathrm{ex}}(n)\rangle/K$ is constant at K_{ex}/K. Therefore, due to the constant accessibility, the probability of an exit site to be occupied increases linearly with the occupancy, then the probability of two adjacent exit sites to be both occupied during propagation is also linearly increasing, therefore the D_0^{mf} trend is expected to be approximately a linear, decreasing function of $\langle n\rangle$.

If the inner sites are set as slightly deeper than the exit sites [e.g., the case of $\Delta f^o=5$ kJ mol^{-1} in Figs. 2(j)–2(l)], then the exit sites accessibility exhibits a slightly increasing trend from values between 0.1 and 0.2 at $n=0$ to K_{ex}/K at $n=K$. This produces a slight inflection of D_0^{mf} at the lowest loadings because is induced a promotion mechanism which

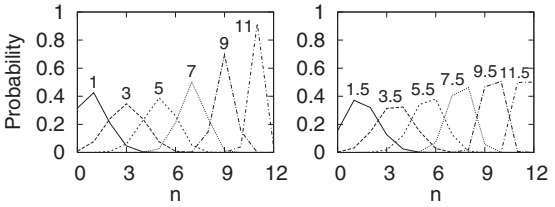

FIG. 3. Occupancy probability distributions for the same system of Fig. 2. Each curve refers to a particular value of the loading $\langle n \rangle$ specified on its top. Distributions for integer and half-integer loadings are shown, respectively, on the left and on the right part of the figure.

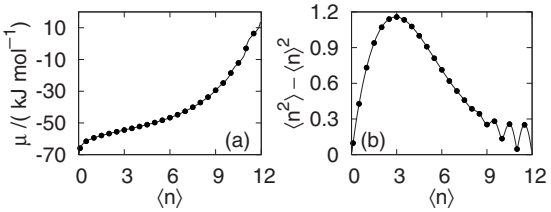

FIG. 4. (a) Chemical potential and (b) variance of the occupancy probability distribution **p** for the same system of Fig. 2.

causes the particles to stay preferentially in the inner sites lowering the probability of two adjacent exit sites to be both occupied.

Finally, when the inner sites are much deeper than the exit sites [e.g., the case of $\Delta f^o = 10$ kJ mol^{-1} in Figs. 2(j)–2(l)], then (i) low values of D_s^{mf} are expected for low loadings due to the fact that at the lowest occupancies most of the occupying particles are located in the inner sites so that the exit sites are poorly occupied and the intercell transfers are rare, (ii) an increase in D_s^{mf} is expected at intermediate-high loadings where almost all the inner sites are occupied and the particles start filling the exit sites, and (iii) a maximum and then a rapid decrease are expected at higher loadings, where exit sites start being saturated, because at the propagation steps become frequent events in which both communicating exit sites of a pair of neighboring cells are occupied.

As mentioned above, in each D_s^{mf} plot of Fig. 2, two self-diffusivity trends are shown for each reported value of Δf^o. Solid and dashed lines represent D_s^{mf} trends obtained, respectively, with and without the inclusion of the kinetic barrier ϵ_{ki} introduced in Paper I.[30] The dashed line exhibits local D_s^{mf} maxima at the highest loadings. This is an effect of the repulsive part of the interaction function $\varepsilon^{\mathrm{pp}}(n)$ at high occupancies. The reason can be found in the propagation probability defined in Paper I,[30] which favors migration events followed by a decrease in free energy. Moreover the positions of the D_s^{mf} peaks at high loadings are remarkable, since they are located at half-integer values of $\langle n \rangle$. They can exist only if in the occupancy probability distribution $p(n)$ there are at least two occupancies much more probable than all the others. In the case of the current parametrization, the shape of $p(n)$ is shown in Fig. 3 for integer (left) and half-integer loadings (right).

At integer loadings the peak in $p(n)$ corresponds to the occupancy $n_{\max} = \langle n \rangle$ and is much more pronounced than all other occupancies. At half-integer loadings instead *two* occupancies (i.e., the ones located around $n_1 = \langle n \rangle - \frac{1}{2}$ and $n_2 = \langle n \rangle + \frac{1}{2}$) are much more probable than all the others. An estimation of the fluctuation of the cell occupancy around its average value is extremely important to characterize the equilibrium properties of the system, since it is a static property strictly related to the first derivative of the adsorption isotherm and, indeed, provides information about the degree of local density heterogeneity in the lattice. The decay of its dynamic counterpart, the autocorrelation function of occupancy fluctuations, is an important time-dependent peculiarity of the host-guest system, and can show a complex behavior.[24] In our model, such a dynamic property is strictly connected with the cell microdynamics.[6] The memory effects in it are due to collective motions of the guests involved in each cell and its respective neighborhood. Although they are averaged out in the calculation of the static occupancy fluctuations, an increase in the complexity of the lattice microdynamics will result in an increasingly complex decay. An investigation of such a feature of our PCA requires a separate study, and will be the subject of a forthcoming paper.

The shape of the free energy interaction term $\phi^{\mathrm{Ay}}(n)$ shown in Fig. 2 favors jumps from a more to a less occupied cell. Therefore at high integer loadings, migrations from a $n_{\max}$-occupied to less occupied cells will happen with a high probability, while the reverse jumps (and all jumps to more occupied cells) will be more rarely observed. The number of migrations per time step will be much lower than in the case of high half-integer loadings, where not only migrations from n_1- and n_2- to less-occupied cells are favored, but also exchanges between n_1- and n_2-occupied cells become very frequent thus producing the diffusivity peaks near the saturation limit. Of course such a behavior is enhanced by irregularities in the chemical potential and occupancy variance trends, which in the parametrization by Ayappa[8] are present and shown in Fig. 4.

B. Correlated motion

The following results illustrate the correlation effects induced by the jump randomization operator $\mathcal{R}^{\mathrm{jump}}$ (see Paper I).[30] To get accurate statistical averages, all simulations were performed on a grid of $16 \times 16 \times 16$ cells for an observation time of 10^5 time steps. Anyway, equilibrium properties of systems of sizes above $L^3 = 4^3$ have been found to converge to the same values, therefore size effects can be considered unimportant in the cases presented here.

We will investigate several three-dimensional systems characterized by different parameter sets:

- System 1—This is a system of noninteracting particles ($\mathbf{\Phi} = 0$). Each cell has $K_{\mathrm{ex}} = 6$ exit sites with fixed energy $f_{\mathrm{ex}}^o = -10$ kJ mol^{-1}, and $K_{\mathrm{in}} = 9$ inner sites with energy $f_{\mathrm{in}}^o = -20$ kJ mol^{-1}. The jump probability reads then

$$p_{\mathrm{jump}}^R(\mathbf{s} \to \mathbf{s}') = A_{jk} e^{\beta f_j^o},$$

where $\mathbf{s} \to \mathbf{s}'$ denotes the change from configuration **s** to $\mathbf{s}'$ caused by a particle jump from site j to site k, the exit-exit jumps are forbidden by means of the same A_{jk}

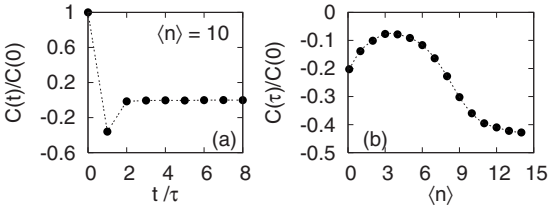

FIG. 5. (a) Displacement autocorrelation function vs time step for loading $\langle n\rangle=10$ and (b) backscattering effect after one time step represented by the ratio $C(\tau)/C(0)$ plotted vs the loading for the system 1.

that we defined in Paper I,[30] and the assumed value of γ is $\exp(-\beta f_{ex})$.

- System 2—Same of system 1 apart from the parameter $\gamma=1$.
- System 3—Same of system 1 apart from

  $p^R_{\text{jump}}(\mathbf{s}\rightarrow\mathbf{s}')=A'_{jk}e^{\beta f^o_j}$,

  where the A'_{jk} (defined in Paper I[30]) allows each jumping particle to choose any of the K cell site during randomization, with $\gamma=\exp(-\beta f_{ex})$.
- System 4—Same of system 3 apart from $\gamma=1$.
- System 5—Same of system 1 apart from $f^o_{ex}=-20$ and $f^o_{in}=-10$, i.e., the depth of the adsorption sites is reversed.
- System 6—System with the same parametrizations as for Fig. 2.

The entity of correlations is well represented by the displacement autocorrelation function (DACF) of a single particle,

$$C(t)=\langle\delta\mathbf{r}(t)\cdot\delta\mathbf{r}(0)\rangle, \tag{34}$$

which has been introduced in Eq. (12). From Fig. 5(a), where the DACF is pictured for loading $\langle n\rangle=10$, it is clear the predominant role played in the entire particle's motion history by the correlation after *one* time step. The ratio $C(\tau)/C(0)$ plotted in Fig. 5(b) expresses the loss of self-diffusivity due to the backscattering effect after one time step. From the reported results we observe a clear loading dependence of the backscattering effect. It is less effective until the system crosses a threshold $[3<\langle n\rangle<4$ in the case of Fig. 5(b)], where due to a decrease in the probability of the particles to find empty sites to jump in during randomization, the trend reverses. In general at loading higher than $\langle n\rangle=K_{in}$ most of the inner sites are occupied. This means that many successful events of migration at time t are ineffective due to the reduced availability of empty sites to jump in during randomization at time $t+\tau$. This causes the particle to have a high probability to return back to the departure cell, so that $C(\tau)/C(0)$ in Fig. 5(b) becomes more negative.

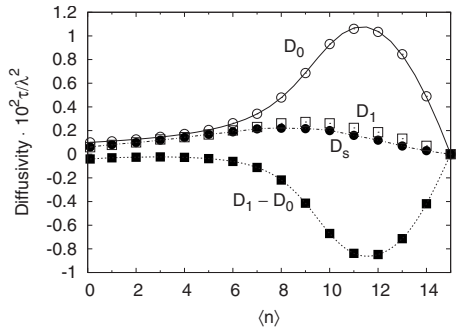

FIG. 6. Self diffusivity profile D_s (black circles) for the system 1 plotted vs the loading together with the zero-time diffusivity D_0 (white circles), the diffusivity after one time step D_1 (white squares), and the backscattering contribution after one time step D_1-D_0 (black squares). The continuous line is the mean-field memoryless diffusivity D_0^{mf}, Eq. (15). Dotted lines are to guide the eyes.

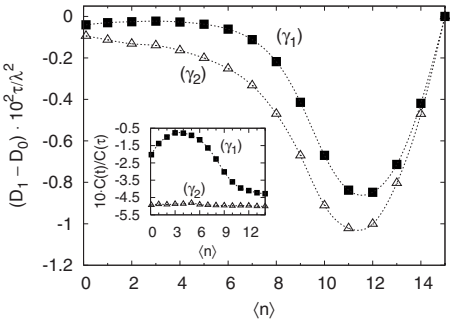

FIG. 7. Backscattering contribution D_1-D_0 vs loading for two different values of γ. Here, $\gamma_2<\gamma_1$ (where γ_1 refers to system 1 and γ_2 to system 2). Dotted lines are to guide the eyes.

It shall be useful to define the diffusivity after j time steps as

$$D_j=\sum_{z=0}^{j}\frac{\langle\delta\mathbf{r}(z\tau)\cdot\delta\mathbf{r}(0)\rangle}{d\tau}-\frac{\langle\delta\mathbf{r}(0)\cdot\delta\mathbf{r}(0)\rangle}{2d\tau}. \tag{35}$$

In Fig. 6 the zero-time diffusivity D_0, the one-time diffusivity D_1, the self diffusivity D_s given in Eq. (14), and the backscattering contribution to the diffusivity after one time step $D_1-D_0=\langle\delta\mathbf{r}(\tau)\cdot\delta\mathbf{r}(0)\rangle/d\tau$ are plotted versus the loading to get a precise idea of the variation in diffusivity caused by the backscattering effect in system 1, where the inner sites are the deepest (i.e., $f^o_{ex}>f^o_{in}$). The mean-field diffusivity computed through Eq. (15) exactly coincides with D_0 by definition. The one-time correlation due to the backscattering effect is most of the total correlations in the motion at least in this case, so that $D_1\approx D_s$.

The effect of reducing the value of γ to 1 is an increase in correlation effect. This is shown in Fig. 7 where the backscattering contribution after one time step D_1-D_0 is more pronounced (i.e., more negative) for the case of $\gamma_2=1$ rather than $\gamma_1=\exp(-\beta f_{ex})$. Moreover, the use of low values of γ (i.e., high jump barrier during randomization) causes correlations to level off, as can be seen in the inset of Fig. 7, where it is shown that the ratio $C(\tau)/C(0)$ becomes less loading-dependent as we lower the value of γ.

The change in shape of the D_s versus $\langle n\rangle$ becomes dramatic when the exit sites are the deepest (i.e., $f^o_{ex}<f^o_{in}$). This can be seen in Fig. 8(a) where the tendency of a particle to *escape* a cell, D_0, is counterbalanced by a backscattering effect, D_1-D_0, almost equal in modulus and with opposite sign. This is confirmed in the $C(\tau)/C(0)$ plot in Fig. 8(b), where the action of the backscattering with respect to the

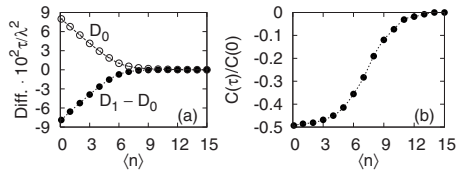

FIG. 8. (a) Zero-time diffusivity, D_0, compared to the backscattering contribution, D_1-D_0, and (b) Normalized DACF $C(t)/C(0)$ for system 5.

escape ability is very important at low loadings [large negative values of $C(\tau)/C(0)$] and decreases with increasing loading until for a highly dense system it becomes null $(C(\tau)/C(0)\approx 0)$. Moreover, the present case remarkably differs from the case of $f_{ex}^{o}>f_{in}^{o}$. The diffusing particle finds itself very often caged inside an exit site during randomization at time t. During propagation it migrates and is again caged into the destination exit site in the next randomization at time $t+\tau$, and so on cyclically until it reaches a sufficient energy to perform a displacement during one of the subsequent randomizations. Such a "rebound process" causes the approximation $D_1\approx D_s$ to be no longer valid. Higher moments of D_j become important, so that a large number of time steps is necessary to define precisely the trend of D_s, as can be seen in Fig. 9. Therefore, the resulting trend of D_s appears very different from D_0 since it exhibits a maximum at low-intermediate loading. This is due to the fact that the rebound process becomes weaker while increasing the loading, since more frequently the particles in the exit sites stop rebounding because of one of the involved exit sites being filled by another particle. This causes the correlations to weaken producing an initial diffusivity increase, which for higher loadings is canceled by the repulsion effect during propagation.

One of the most realistic phenomena induced by the jump randomization is the differentiation between the *self* and the *collective* diffusivity,[25] the latter quantity being defined as

$$D_c=\frac{N}{2d}\lim_{t\to\infty}\frac{\langle[\Delta\mathbf{r}_{CM}(t+\tau)]^2\rangle-\langle[\Delta\mathbf{r}_{CM}(t)]^2\rangle}{\tau}, \tag{36}$$

where $\Delta\mathbf{r}_{CM}(t)=\mathbf{r}_{CM}(t)-\mathbf{r}_{CM}(0)$ with $\mathbf{r}_{CM}(t)$ as the coordinates of the center-of-mass at the time t. Equation (36) can be expanded as a function of the displacement mixed-correlation function (DMCF) $\langle\delta\mathbf{r}_i(t)\cdot\delta\mathbf{r}_j(t')\rangle$, where $\delta\mathbf{r}_i(t)$ is

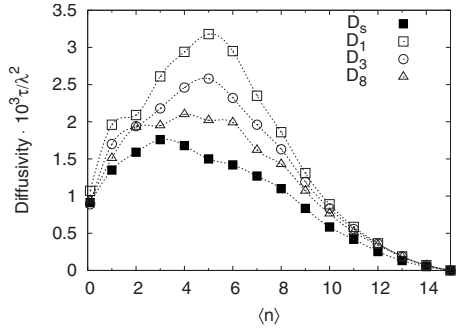

FIG. 9. Self diffusivity profile D_s vs loading for the system 5, plotted together with the diffusivity after 1, 3, and 8 time steps. Dotted lines are to guide the eyes.

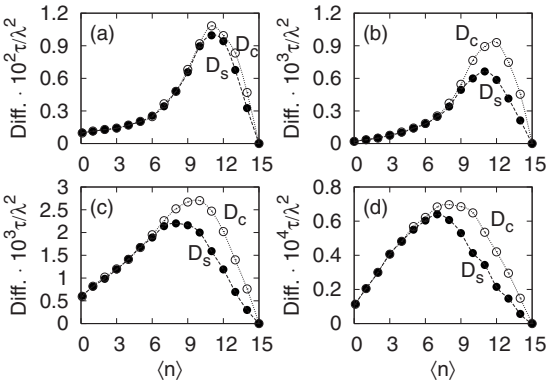

FIG. 10. Self and collective diffusivity for (a) system 3, (b) system 4, (c) system 1, and (d) system 2.

the instantaneous cell-to-cell displacement function, Eq. (10), for the ith particle obtaining

$$D_c=D_0+\frac{1}{d\tau}\sum_{z=1}^{\infty}\langle\delta\mathbf{r}(z\tau)\cdot\delta\mathbf{r}(0)\rangle+\frac{1}{2d\tau N}\sum_{\substack{1\le i,j\le N\\ i\neq j}}\left\{\langle\delta\mathbf{r}_i(0)\cdot\delta\mathbf{r}_j(0)\rangle+2\sum_{z=1}^{\infty}\langle\delta\mathbf{r}_i(z\tau)\cdot\delta\mathbf{r}_j(0)\rangle\right\}, \tag{37}$$

where the sum of the first two terms gives the self-diffusivity, and the last sum incorporates all contributions arising from correlations between the displacements of all possible pairs of particles in the system. In Eq. (37) all contributions arising from both self-and mixed-correlations are present. Details about the derivation of Eq. (37) can be found in Appendix B.

If the randomization is memoryless, then the migration process is governed only by the ability of particles to escape from their host cell. Therefore in that case, neither correlation in the self-motion nor in the collective motion is expected,[6] since the mixed displacement correlations for different particles cancel out.

In the case of jump randomization, some correlations between different particles will cancel out with some correlations in the self-motion, and this will result in a D_c slightly higher than D_s. This is shown in Figs. 10 and 11, where D_s and D_c trends are compared directly, respectively, for the noninteracting and the interacting case. It should be noticed that in all these cases the difference between D_c and D_s increases in those regions where the migration sites are more involved in the migration process than the inner sites (i.e., from low to intermediate loadings if the exit sites are the deepest, and from intermediate to high loadings if the inner sites are the deepest). By comparison of the trends in Figs. 10 and 11 with the plots of collective-and self-diffusivity obtained from molecular dynamics simulation (see, e.g., Dubbeldam *et al.*[13] for the case of methane in ZK4), we conclude that the local, discrete rules developed in the present work effectively capture the most relevant aspects of diffusion of simple chemical species in zeolites.

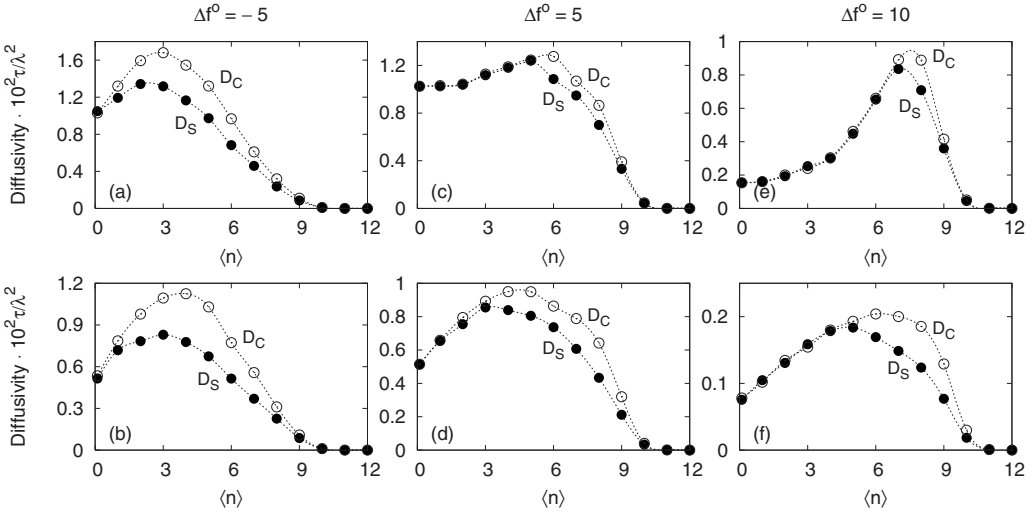

FIG. 11. Self and collective diffusivities for the same system of Fig. 2, while using the jump randomization. In figures (a), (c), and (e) jumps among different exit sites are allowed during randomization. In figures (b), (d), and (f) instead, such jumps are not allowed. Dotted lines are to guide the eyes.

V. CONCLUSIONS

These two papers conclude the theoretical development of our PCA designed to faithfully capture the nature of sorption and diffusion in microporous solids and to exploit the potential of massively parallel computer architectures. The physics content of the model straightly springs from structure and sorption properties of molecules confined in a zeolite crystal, mainly looking at the basic links between atomistic-scale processes and mesoscopic behavior. With respect to our previous lattice gas CA[5,6] we added the action of local guest-guest interactions and proved how synchronicity in the evolution rule can be preserved by adopting the Block CA (BCA) approach introduced by Toffoli and Margolous.[26,27] The microscopic evolution of our PCA satisfies the balance conditions as illustrated in Paper I,[28–30] while in this paper we tested two randomization schemes: the former which destroys the correlations in the particle's motion and the latter which produces a correlated self-motion of the particles. We presented a mean-field theory of the single cell model at equilibrium followed by a detailed description of the procedure we propose to calculate the chemical potential, while working in the Canonical Ensemble. The in-deep investigations on the correlated motions reveal the flexibility of the model we are proposing and especially its ability in reproducing transport properties. In conclusion, it is appropriate to remark that the model is adaptive to the type of the available reference data. In our previous work[17] we have shown that a *top-down* strategy can be adopted when data from experiments or atomistic simulation over a small system can be collected to obtain the saturation occupancy K, and to find the best parameter set giving the correct chemical potential and diffusion behavior. A *bottom up* strategy can also be developed *ad hoc* for each host-guest system under study, aimed to derive from microscopic simulations the distribution of molecules in the regions close to the windows inside of each pore to get: energy parameters, local transfer rates, and to estimate the entity of memory effects. This will be the subject of a forthcoming paper. Moreover we note that our PCA is quite general and can be easily extended to various zeolite topologies as well as other research fields involving local systems weakly coupled with one another, able to exchange energy and/or matter at relatively low rate whenever it is required an effective sampling of large length and time scales.

ACKNOWLEDGMENTS

This work has been carried out with financial support provided by Italian Ministero dell'Istruzione, dell'Università e della Ricerca, by Università degli Studi di Sassari, and by Istituto Nazionale per la Scienza e Tecnologia dei Materiali (INSTM), which are acknowledged.

APPENDIX A: THE TIME STEP

Usually CA evolve in time according to their own internal clock, usually referred to as a parameter τ, which is homogeneous, and in our PCA approach also *independent of the loading* $\langle n \rangle$. In principle, τ is a free time parameter, and since it does not enter in the evolution algorithm the trends of the dynamical properties arising from the CA evolution are not affected by its numerical value, instead they are just scaled by a factor τ. In other words, when expressed in units of time steps (instead of seconds) the dynamical properties of a CA do not depend on τ.

Anyway, the time step τ cannot be assigned an arbitrarily large value, since it appears in the denominator in the right-hand side of Eq. (13) as the time interval of the discrete-time derivative of the function $\langle [\Delta \mathbf{r}(t)]^2 \rangle$. In order to get an idea of the order of magnitude of τ, it should be noted that the evolution algorithm is devised in such a way that, during one time step, a particle can migrate at most into one of the first-neighbors of the leaving cell. Therefore, the numerator of the derivative, $\langle [\Delta \mathbf{r}(t+\tau)]^2 \rangle - \langle [\Delta \mathbf{r}(t)]^2 \rangle$, is of the order of λ^2 (with λ the cage-to-cage distance of the simulated zeolitic structure), and τ is constrained to be not greater than the mean time required to a (real) sorbate molecule to migrate from a cage to a neighboring one in an atomistic simulation. Then, a value for τ in units of real time can be conveniently

defined as the ratio between the self-diffusivity of the PCA, expressed in units of length^2/time-step-unit, and the self-diffusivity of the reference system, expressed in units of length^2/real-time-unit in the limit of zero loading. By this way the PCA can be modeled in order to achieve quantitative agreement between the dynamical properties of the automaton and of a reference system, which might be, e.g., data from molecular dynamics simulations or experimental results. We note that from a PCA simulation the self-diffusivity we compute directly is not D_s [see Eqs. (13) and (14)], but D_s^{int} instead, which is the self-diffusivity in internal units, given by

$$D_s = \frac{\lambda^2}{\tau} D_s^{\text{int}}, \tag{A1}$$

where λ is the lattice spacing (the cage-to-cage distance in the zeolite). Then τ can be formulated as

$$\tau = \frac{\lambda^2 \lim_{\langle n\rangle \to 0} D_s^{\text{int}}}{\lim_{\langle n\rangle \to 0} \mathcal{D}_s}, \tag{A2}$$

where $\mathcal{D}_s$ is the reference self-diffusivity, in units of m^2 s^{-1}.

However this is not the only way τ can be defined. As example, τ could be assumed to be a loading-dependent parameter, so that the correspondence between the diffusivities of PCA and of reference system would have to be built for every different value of $\langle n\rangle$. However, for simplicity and for consistence with the CA philosophy, τ has been assumed to be loading-independent. In this way, the refinement of the dynamic behavior can be accomplished by modeling the *local* kinetic parameter,[17] ϵ_{ki}, and the memory effects, without invoking any further assumption for τ.

APPENDIX B: COLLECTIVE DIFFUSION COEFFICIENT

Since the coordinates of the center-of-mass at time t are given by

$$\mathbf{r}_{\text{CM}}(t) = \frac{1}{N}\sum_{i=1}^{N} \mathbf{r}_i(t), \tag{B1}$$

the center-of-mass displacement at time t is

$$\Delta\mathbf{r}_{\text{CM}}(t) = \mathbf{r}_{\text{CM}}(t+\tau) - \mathbf{r}_{\text{CM}}(t) = \frac{1}{N}\sum_{i=1}^{N}\sum_{z=0}^{Z-1} \delta\mathbf{r}_i(z\tau), \tag{B2}$$

where $Z = t/\tau$ is the number of time steps needed for the system to evolve from time 0 to time t, and $\delta\mathbf{r}_i(z\tau)$ is the instantaneous cell-to-cell displacement function, Eq. (10) for the ith particle. The mean-squared center-of-mass displacement results therefore

$$\begin{aligned}\langle[\Delta\mathbf{r}_{\text{CM}}(t)]^2\rangle &= \frac{1}{N^2}\left\langle \sum_{i=1}^{N}\sum_{j=1}^{N}\sum_{z=1}^{Z-1}\sum_{w=1}^{Z-1} \delta\mathbf{r}_i(z\tau)\cdot\delta\mathbf{r}_j(w\tau)\right\rangle \\ &= \frac{1}{N^2}\sum_{i=1}^{N}\sum_{j=1}^{N}\left\{ Z\langle\delta\mathbf{r}_i(0)\cdot\delta\mathbf{r}_j(0)\rangle \right. \\ &\quad \left. + 2\sum_{z=1}^{Z-1}(Z-z)\langle\delta\mathbf{r}_i(z\tau)\cdot\delta\mathbf{r}_j(0)\rangle\right\}. \end{aligned} \tag{B3}$$

The instantaneous variation of the average center-of-mass displacement results

$$\begin{aligned}&\langle[\Delta\mathbf{r}_{\text{CM}}(t+\tau)]^2\rangle - \langle[\Delta\mathbf{r}_{\text{CM}}(t)]^2\rangle \\ &= \frac{1}{N^2}\sum_{i=1}^{N}\sum_{j=1}^{N}\left\{\langle\delta\mathbf{r}_i(0)\cdot\delta\mathbf{r}_j(0)\rangle \right. \\ &\quad \left. + 2\sum_{z=1}^{Z}\langle\delta\mathbf{r}_i(z\tau)\cdot\delta\mathbf{r}_j(0)\rangle\right\}, \end{aligned} \tag{B4}$$

$$\begin{aligned}&= \frac{1}{N}[\langle[\Delta\mathbf{r}(t+\tau)]^2\rangle - \langle[\Delta\mathbf{r}(t)]^2\rangle] \\ &\quad + \frac{1}{N^2}\sum_{\substack{1\le i,j\le N\\ i\neq j}}\left\{\langle\delta\mathbf{r}_i(0)\cdot\delta\mathbf{r}_j(0)\rangle \right. \\ &\quad \left. + 2\sum_{z=1}^{Z}\langle\delta\mathbf{r}_i(z\tau)\cdot\delta\mathbf{r}_j(0)\rangle\right\}, \end{aligned} \tag{B5}$$

where in the last equality, Eq. (B5), we have separated the self-term from the mixed terms, and $\langle[\Delta\mathbf{r}(t+\tau)]^2\rangle$ is given in Eq. (12) Application of Eq. (36) gives the expression for the collective diffusivity in terms of the DMCF, Eq. (37).

[1] B. Chopard and M. Droz, *Cellular Automata Modeling of Physical Systems* (Cambridge University Press, Cambridge, England, 1998).
[2] J. P. Boon, D. Dab, R. Kapral, and A. T. Lawniczak, Phys. Rep. **273**, 55 (1996).
[3] J.-P. Rivet and J. P. Boon, *Lattice Gas Hydrodynamics* (Cambridge University Press, Cambridge, England, 2001).
[4] P. Demontis, F. G. Pazzona, and G. B. Suffritti, J. Phys. Chem. B **110**, 13554 (2006).
[5] P. Demontis, F. G. Pazzona, and G. B. Suffritti, J. Chem. Phys. **126**, 194709 (2007).
[6] P. Demontis, F. G. Pazzona, and G. B. Suffritti, J. Chem. Phys. **126**, 194710 (2007).
[7] T. T. P. Cheung, J. Phys. Chem. **97**, 8993 (1993).
[8] K. G. Ayappa, J. Chem. Phys. **111**, 4736 (1999).
[9] C. Saravanan, F. Jousse, and S. M. Auerbach, Phys. Rev. Lett. **80**, 5754 (1998).
[10] M.-O. Coppens, A. T. Bell, and A. K. Chakraborty, Chem. Eng. Sci. **54**, 3455 (1999).
[11] C. Tunca and D. Ford, Chem. Eng. Sci. **58**, 3373 (2003).
[12] R. Krishna, D. Paschek, and R. Baur, Microporous Mesoporous Mater. **76**, 233 (2004).
[13] D. Dubbeldam, E. Beerdsen, T. J. H. Vlugt, and B. Smit, J. Chem. Phys. **122**, 224712 (2005).
[14] D. A. McQuarrie, *Statistical Mechanics* (Harper & Row, New York, 1976).
[15] R. Brito, H. J. Bussemaker, M. H. Ernst, and J. Matsui, Phys. Rev. E **52**, 2657 (1995).
[16] B. Widom, J. Chem. Phys. **39**, 2808 (1963).
[17] P. Demontis, F. G. Pazzona, and G. B. Suffritti, J. Phys. Chem. B **112**, 12444 (2008).
[18] C. J. Jameson, A. K. Jameson, B. I. Baello, and H.-M. Lim, J. Chem. Phys. **100**, 5965 (1994).
[19] A. K. Jameson, C. J. Jameson, and R. E. Gerald II, J. Chem. Phys. **101**, 1775 (1994).
[20] R. S. Drago, C. E. Webster, and J. M. McGilvray, J. Am. Chem. Soc. **120**, 538 (1998).
[21] W. Zhu, F. Kapteijn, and J. A. Moulijn, Phys. Chem. Chem. Phys. **2**, 1989 (2000).
[22] A. J. Skoulidas and D. S. Sholl, J. Phys. Chem. A **107**, 10132 (2003).

[23] P. Demontis and G. B. Suffritti, J. Phys. Chem. B **101**, 5789 (1997).
[24] P. Demontis, L. Fenu, and G. B. Suffritti, J. Phys. Chem. B **109**, 18081 (2005).
[25] B. Smit and T. L. M. Maesen, Chem. Rev. (Washington, D.C.) **108**, 4125 (2008).
[26] T. Toffoli and N. Margolus, Physica D **45**, 229 (1990).
[27] T. Toffoli and N. Margolus, *Cellular Automata Machines: A New Environment for Modeling* (MIT, Cambridge, MA, 1997).
[28] V. I. Manousiouthakis and M. W. Deem, J. Chem. Phys. **110**, 2753 (1999).
[29] D. Frenkel and B. Smit, *Understanding Molecular Simulations—From Algorithms to Applications*, 2nd ed. (Academic, New York, 2002).
[30] F. G. Pazzona, P. Demontis, and G. B. Suffritti, J. Chem. Phys. **131**, 234703 (2009).